Title:

Characteristics of Sea Ice Floe Size Distribution in the Seasonal Ice Zone

Takenobu Toyota[1], Shinya Takatsuji[2] and Masashige Nakayama[3]

1 Institute of Low Temperature Science

2 Nara Local Meteorological Observatory

3 Kushiro Children's Museum

Running Title:

Ice floe size distribution in the SIZ

Abstract

The size distribution of sea ice floes was observed by coordinated Landsat imagery and video monitoring conducted from an icebreaker and a helicopter for an area 38km× 26km in seasonal sea ice in the southern Sea of Okhotsk in February 2003. The combination of imagery on several scales allowed measurements of ice floes over three orders of magnitude, from 1 m to 1.5 km. Two different regimes were observed: floes larger than about 40 m have a power-law number density with an exponent of -1.87, in the lower range of earlier results. Below 40 m, the power law exponent is -1.15. The cause of these two different regimes is hypothesized to lie in the effects of swell on floes of different sizes and thicknesses. The importance of the floe size distribution for lateral melting is elucidated.

1. Introduction

In the seasonal ice zones (SIZ), various types of ice floes are present, and their sizes range from about one meter to kilometers. Commonly, the present numerical model of sea ice treats two variables, ice concentration and thickness, to represent these ice states. However, the response to wind and melting depends on ice floe size, and the floe size distribution can also be one of the important ice state variables. Steele et al. [1989] pointed out that ice velocity significantly decreases for ice floes smaller than about 100 m in diameter due to the form drag effect. Further, Steele [1992] showed that the melting rate of ice floes significantly increases for floe sizes smaller than about 30 m because lateral melting becomes more prominent for smaller ice floes. Therefore, it can be said that in the SIZ, where most ice floes are small, the ice floe distribution is a key parameter for both dynamics and thermodynamics. In addition, the size and shape distributions of floes possibly provide a clue to the understanding of ice floe formation processes. Generally a magnified image of part of an ice area looks almost identical to the original image. That is, the floe distribution appears to have a self-similar property. If this is confirmed quantitatively, it may have implications on the formation process of ice floes.

So far, several researchers have addressed this issue. For the Beaufort, Chukchi, and East Siberian Seas, the floe size distribution was investigated by Weeks et al. [1980] with airborne side-looking radar data, by Rothrock and Thorndike [1984] with aerial photographic mosaics and Landsat imagery, and by Holt and Martin [2001] with ERS-1/SAR imagery. Their analyses show that the cumulative number distribution $N(d)$,

the number of floes per unit area with diameters no smaller than d, behaves like $d^{-\alpha}$, $1.7 < \alpha < 2.9$. For the Sea of Okhotsk, Matsushita [1985] and Toyota and Enomoto [2002] also showed with satellite imagery that the floe size distribution obeys $N(d) \propto d^{-\alpha}$, $2.1 < \alpha < 2.5$. These results indicate that these floe size distributions in the SIZ are basically self-similar. However, all these analyses focused on ice floes larger than 100 m and little is known about ice floes smaller than 100 m. Although Inoue et al. [2004] indirectly estimated the size distribution of ice floes smaller than 100 m with airborne video imagery, they did not treat individual ice floes. Moreover, the problem is that the exponent α often exceeds 2 in the past results. Mathematically, α must be less than 2 for small ice floes, otherwise the ice area would become infinite [Rothrock and Thorndike, 1984]. This suggests that the size distribution must change for floes smaller than 100 m, and therefore an analysis including floes size down to meters, is desirable. For this purpose, we conducted in-situ observations in the southern Sea of Okhotsk and analyzed floes ranging from 1 m to 1.5 km with imagery from ship-borne and heli-borne video cameras and from Landsat. The purpose of this study is to examine the ice floe distribution in this region and then to determine the statistical characteristics, which may serve to shed light on the ice floe formation process.

2. Measurement

The in-situ observations were conducted with an icebreaker P/V “Soya” on February 11, 2003, coordinated with a Landsat-7 overpass. The study area is shown in Figure 1. Along the cruise track, ice conditions were monitored at different altitudes

with ship-borne and heli-borne video cameras. The individual tracks are shown in Figure 1a. Four rectangular regions with sides of 19 km and 13 km containing the cruise track were selected from the original scene of Landsat-7/ETM+ for analysis. The weather was clear and cloud free. Although the cruise track covers only a limited part of satellite imagery, it seems to be approximately representative.

A ship-borne video camera was installed on the ship's mast at a height of 19 m above the sea level and monitored ice conditions ahead of the ship. The video images were taken from an oblique angle, so reprocessing was needed before floe analysis. Here, we used a one-dimensional analysis method. First, we set a fixed row around the center of video images so that sea ice is clearly recognized and the width is long enough (60 m) on the row. As the ship proceeded, we sampled the brightness data on that row and then aligned them in temporal order, which gives us a picture as if it were taken from the air. The sampling interval was 1/30 sec. For convenience, each picture was renewed at the interval of 5 minutes (corresponding to about 1.5 km). Since there are 700 pixels in each row, one pixel represents about 9 cm. The interval between rows is estimated from ship speed to be about 15 cm. Thus, the horizontal resolution of this dataset is about 10 cm. The error caused by the freeboard of ice floes seems to be trivial, mostly less than 10 cm.

Heli-borne video images were taken at altitudes of 180, 440, 730, and 1300 m. The individual tracks were the same as the ship's. At each altitude, the ice conditions right below were recorded. Among these the 440 and 1300 m level data were used here to complement the ship-borne and satellite imagery. The widths of the image are

estimated to be 180 m and 430 m, and the horizontal resolutions are about 0.4 m and 1.3 m. During the flight, the altitudes fluctuated slightly from the nominal levels with the standard deviations of 11.3 m (at 440 m altitude) and 8.8 m (at 1300 m). However, it does not seem to be vital, because the error due to this fluctuation is only 1 to 3 % of the floe size. To provide for efficient floe analysis, consecutive video images taken every 1/30 sec. were integrated into a composite picture by merging the images at the best fitted point, using the method developed by Oda et al. [1998]. For convenience, each picture was renewed every one minute, corresponding to about 3 km in length.

3. Floe Analysis

The procedures of analysis are basically the same for the three kinds of dataset. By means of image processing, each sea ice floe was extracted according to its brightness, and then its area (S) was measured. In this study, floe size (d) is evaluated as the diameter of a circle that has the same area as that of the floe: $d=(4S/\pi)^{1/2}$. For heli-borne video and Landsat imagery, the perimeter and maximum/minimum caliper diameters (d_{max}/d_{min}) were also measured to examine the shape properties of ice floes. Here a caliper diameter is the size of opening through which the floe may pass in a particular orientation. For the video imagery, the ship speed was also taken into account to calculate the floe area.

In this analysis, the most important but difficult task is to precisely determine the edges of ice floes. Here, the difference of brightness between water and sea ice was used in principle. To do this quantitatively, the RGB color brightness of each pixel was

converted into grey scale (L) by L=0.3R+0.59G+0.11B: 0<R,G,B<4095, then 0<L<4095 as well. To strengthen the contrast, the highest (lowest) 3% pixels of L within one image were replaced by 4095 (0), and then the grey scales (L') of the remaining pixels were interpolated linearly between these two levels. With these grey scaled images, the edge of each ice floe was determined according to the following procedure: first, based on the histogram of L' for each image, the threshold which separates ice floe from water was determined. In most cases, the histogram shows a bimodal distribution in correspondence to water and ice floes (Figure 2a). The local minimum brightness (B_{min}) between these two peaks could be a threshold. This, however, sometimes failed in extracting ice floes one by one when they are closely distributed. Therefore the threshold should be somewhat higher than B_{min}. On the other hand, as it becomes higher, the shadow on the floes made by ridged ice tends to be categorized into water. By comparing with the visual floe pattern on the images, the brightness obtained by adding 0.3×(maximum brightness (4095) - B_{min}) to B_{min} was adopted as a threshold. This method allowed us to efficiently extract numbers of ice floes, but did not work well when ice floes were directly in contact with the neighboring floes, as in the blue circles in Figure 2b. In such cases, we manually corrected the edge lines so that each floe is basically convex and matches the visual floe pattern as much as possible. Ice that crosses the boundary of the region or appears to be smaller than the resolution of the image was excluded from the analysis. The numbers of floes analyzed from ship-borne video images, 440-m heli-borne video images, 1300-m video images, and Landsat images were 7,331, 19,847, 14,803, and 29,612.

4. Results

Following Rothrock and Thorndike [1984], the results for each dataset are represented in the form of cumulative number distributions $N(d)$. It should be noted that each dataset has a suitable scale for analysis according to its pixel size and areal coverage. The lower limit should be a few times the pixel size, that is, 0.3 m for ship data, 1.3 m and 4 m for the two altitudes of heli data, and 80 m for Landsat data. Although the upper limit of the suitable scale was not determined, the value from higher altitude was adopted preferentially if $N(d)$ was duplicated between different datasets for the same diameter. This is because the imagery from a higher altitude contains a larger number of floes and is more representative.

Figure 3 shows the cumulative number distribution obtained through these procedures. The log-log graph has two slopes with a transition zone at a diameter of about 40 m, indicating that $N(d)$ behaves like $d^{-\alpha}$ within each slope range. The exponent α is estimated by the least squares method to be 1.87 for floes larger than 40 m and 1.15 for floes smaller than 40 m. Although the first value is less than 2 and the result of $2.1 < \alpha < 2.5$ [Toyota and Enomoto, 2002], it is within the range of the earlier results for ice floes larger than 100 m [e.g., $1.7 < \alpha < 2.5$ by Rothrock and Thorndike, 1984] and is consistent with the past research. Of importance is the result that α decreases to significantly below 2 for smaller ice floes. This result solves the “infinite area” problem mentioned in section 1. Further, this also suggests that the processes of ice floe formation are different for different floe sizes. In Figure 3, the slope decreases significantly again below 1 m, but this does not seem to be meaningful. This is because

at this size most ice floes belong to brash ice in irregular shapes, and it is almost impossible to extract them accurately.

Next, we would like to mention the shape of ice floes. Here, we define the diameter (d_p), defined by that of a circle which has the same perimeter as the floe: $d_p=P/\pi$, where P is the floe perimeter. When the ratio of d_p to d is unity, the shape should be exactly a circle. The greater the ratio becomes, the more distorted the shape becomes from a circle. Therefore, this ratio is regarded as a parameter of the degree of distortion. Figure 4a shows the relationship between d and d_p for all the ice floes analyzed. It is noticeable that they are almost linearly correlated and the ratio is estimated as 1.145 ± 0.002 with the 95% significance level. This value is somewhat lower than 1.29 by Toyota and Enomoto [2002] and close to 1.11 estimated from Rothrock and Thorndike [1984]. If we assume ice floes of elliptical shape, the ratio d_p/d of 1.145 corresponds to the ellipse whose aspect ratio is 2.4. To examine this more explicitly, the relationship between the maximum and minimum caliper diameters, d_{max} and d_{min}, are also plotted for individual ice floes in Figure 4b. It is shown that they are also correlated, though not so well as d and d_p. The ratio d_{max}/d_{min} is estimated as 1.78 ± 0.4. This value is almost within the range of the result (1.2 to 2.2) obtained for multi-year ice by Hudson [1987]. Consequently, our results show that the ice floes have the aspect ratio of around 2 on average and are usually distorted, not of a circular shape. These values are almost the same for the two regimes, suggesting that the property of ice floe shape is almost independent of floe size.

5. Discussion

Here we discuss what caused the two regimes in the size distribution. As for physical processes that determine the floe geometry, Rothrock and Thorndike [1984] pointed out melting of ice floes, failure due to collision of ice floes, and flexural failure by ocean swell. Among these processes, it seems to be the flexural failure by swell that works differently depending on the floe size. Therefore, we focus on the flexural failure due to swell here. Concerning the response of sea ice to swell, Higashi et al. [1982] showed using the general equation of elastic motion that when ice plate is shorter than 100 m, flexural failure becomes relatively difficult with the decrease of ice length for any wave period and amplitude. Meylan and Squire [1994] also showed from a precise linear mathematical theory that the vertical strain of ice floe due to swell decrease much for ice floes smaller than 100 m for any wavelength. This is consistent with our result that the slope of the floe size distribution is gradually reduced below 100 m. In addition, from the viewpoint of the mechanical flexure of ice floes the minimum size of breakup can be estimated as 14, 24, and 33 m for 1, 2, and 3 m thick ice [Mellor, 1986]. This implies that sea ice smaller than about 40 m in diameter can scarcely be broken up mechanically. Thus in the regime of ice smaller than 40 m, the floe size distribution may be determined by the welding of smaller sea ice such as pancake ice, rather than by the breakup due to swell or by uneven melting of larger floes. On the other hand, in the regime of floes larger than 40 m diameter, breakup seems to play an important role as well as welding in determining the ice floe distribution. Between the two regimes, we surmise that the different conditions of swell and ice thickness affect the distribution

and produce the transition zone.

Next we discuss how much influence the size distribution for smaller floes has on a lateral melting process of sea ice. To examine this, we calculate the total perimeter of all the ice floes and compare it with that for the case where there is only one regime. Here let us suppose that the cumulative number distribution be described as $N_a(d) = \beta_1 \cdot d^{-\alpha_1}$ for $d_1<d<d_2$ and $N_b(d) = \beta_2 \cdot d^{-\alpha_2}$ for $d_2<d<d_3$. In this case, the ice concentration A is given by

$$A = \int_{d_1}^{d_2} n_a(x)s(x)dx + \int_{d_2}^{d_3} n_b(x)s(x)dx$$

$$= -\frac{\pi\beta_1\alpha_1}{4(\alpha_1-2)}(d_2^{-\alpha_1+2} - d_1^{-\alpha_1+2}) - \frac{\pi\beta_2\alpha_2}{4(\alpha_2-2)}(d_3^{-\alpha_2+2} - d_2^{-\alpha_2+2})$$

for $\alpha_{1,2} \neq 2$, where $n_{a,b}(x)dx = -\frac{dN_{a,b}(x)}{dx}dx$ are the number of floes whose diameters are x to $x+dx$ per unit area, and $s(x)$ is the area of a floe ($= \pi x^2/4$). From the boundary conditions $N_a(d_2) = N_b(d_2)$, β_1 should be equal to $\beta_2 d_2^{-\alpha_2+\alpha_1}$. With these equations, $\beta_{1,2}$, and then $N_{a,b}(d)$ are determined for the fixed parameters of A, d_1, d_2, d_3, α_1, and α_2. This allows us to calculate the total perimeter of ice floes. Based on our results, we assign the values of 1 m, 40 m, 1500 m, 1.15, and 1.87 to the parameters of d_1, d_2, d_3, α_1, and α_2. In calculation, the ratio d_p/d (=1.145) is also used, and A is assumed to be 0.8. The result is compared with that for only one regime where α_1 and α_2 are both equal to 1.87. Consequently, it is found that the perimeter for two regimes is as much as 4.8 times less than that for only one regime. This result indicates that the

size distribution of ice floes smaller than 40 m has a strong effect on a lateral melting process. Recently the importance of lateral melting has been pointed out from observation for the Antarctic sea ice in melting season [Nihashi et al., 2005] and from numerical simulation for the Sea of Okhotsk even in mid-winter [Watanabe et al., 2004]. Therefore, it appears that taking account of floe size distribution especially for small floes, should significantly improve sea ice models.

In this study, the size distribution of ice floes over three orders of magnitude, from 1 m to 1.5 km, is evaluated for the first time in the SIZ. It is revealed that there are two regimes for floes larger than and below 40 m in diameter and the significant effect on melting is discussed. However, since our study is limited in both time and region, the accumulation of more data is required to enhance our understanding of floe size distribution. To elucidate the effect of lateral melting, further analysis especially in the melting season is desirable in the future.

Acknowledgments

The authors deeply appreciate the support by the crew of P/V Soya, J. Inoue and Y. Mukai during the observation. The editing of the heli-borne video images was conducted by K. Naoki and Prof. F. Nishio. The comments by Profs. N. Ebuchi, M. Wakatsuchi, and H. Mitsudera and critical reading of this manuscript by Prof. H. H. Shen and K. I. Ohshima are also acknowledged. Image processing was carried out using Image Pro Plus ver. 4.0. This study was supported by the fund from Research Revolution 2002 (RR2002) of Project for Sustainable Coexistence of Human, Nature and the Earth of the MEXT of the Japanese Government.

Reference Lists

Higashi, A., D. J. Goodman, S. Kawaguchi, and S. Mae (1982), The cause of the breakup of fast ice on March 18, 1980 near Syowa Station, east Antarctica, *Proceedings of the fourth symposium on polar meteorology and glaciology*, 222-231.

Holt, B., and S. Martin (2001), The effect of a storm on the 1992 summer sea ice cover of the Beaufort, Chukchi, and East Siberian Seas, *J.Geophys.Res., 106*(C1), 1017-1032.

Hudson, R. D. (1987), Multiyear sea ice floe distribution in the Canadian Arctic Ocean, *J.Geophys.Res., 92*(C13), 14,663-14,669.

Inoue, J., M. Wakatsuchi, and Y. Fujiyoshi (2004), Ice floe distribution in the Sea of Okhotsk in the period when sea-ice extent is advancing, *Geophys.Res.Lett., 31*, L20303, doi:10.1029/2004GL020809.

Matsushita, M. (1985), Fractal viewpoint of fracture and accretion, *J.Phys.Soc.Jpn., 54*(3), 857-860.

Mellor, M. (1986), The mechanical behavior of sea ice, in *Geophysics of Sea Ice*, edited by N. Untersteiner, 165-281, Plenum Press, New York.

Meylan, M, and V. A. Squire (1994), The response of ice floes to ocean waves, *J. Geophys. Res., 99*(C1), 891-900.

Nihashi, S., K. I. Ohshima, M. O. Jeffries, and T. Kawamura (2005), Sea-ice melting processes inferred from ice-upper ocean relationships in the Ross Sea, Antarctica, *J.Geophys.Res., 110,* C02002, doi:10.1029/2003JC002235.

Oda, K., T. Kondoh, M. Obata, T. Doihara (1998), Automated Image mosaicing based on Levenberg-Marquardt method, *J. of Jpn.Soc.of Photogrammetry and Remote Sensing*, *37*(3), 42-51. (in Japanese with English summary)

Rothrock, D. A., and A. S. Thorndike (1984), Measuring the sea ice floe size distribution, *J.Geophys.Res.*, *89*(C4), 6477-6486.

Steele, M. (1992), Sea ice melting and floe geometry in a simple ice-ocean model, *J.Geophys.Res.*, *97*(C11), 17,729-17,738.

Steele, M., J. H. Morison, and N. Untersteiner (1989), The partition of air-ice-ocean momentum exchange as a function of ice concentration, floe size, and draft, *J.Geophys.Res.*, *94*(C9), 12,739-12,750.

Toyota, T., and H. Enomoto (2002), Analysis of sea ice floes in the Sea of Okhotsk using ADEOS/AVNIR images, *Proceedings of the 16th IAHR International Symposium on ice, Dunedin, New Zealand*, 211-217.

Watanabe, T., M. Ikeda, and M. Wakatsuchi (2004), Thermohaline effects of the seasonal sea ice cover in the Sea of Okhotsk, *J.Geophys.Res.*, *109*, C09S02, doi:10.1029/2003JC001905.

Weeks, W. F., W. B. Tucker, M. Frank, and S. Fungcharoen (1980), Characteristics of surface roughness and floe geometry of sea ice over the continental shelves of the Beaufort and Chukchi Seas, In *Sea Ice Processes and Models*, edited by R.S. Pritchard, 300-312, Univ. of Washington Press, Seattle.

Figure Captions

Figure 1: (a) Map of the Sea of Okhotsk with the cruise tracks of the P/V “SOYA” (thin line) and the helicopter (red line).

(b) A Landsat-7/ETM+ image of the solid line area in Fig.1a with parallels and meridians. In the picture, the regions surrounded by thick blue lines are the study area. The horizontal resolution is 15 m. The red line denotes the cruise track, where video monitoring observation was conducted by a helicopter.

Figure 2: One example of analysis.

(a) A histogram of grey scaled brightness (L') with a threshold line.

See the text for the details of the method to determine the threshold.

(b) The ice edges drawn in red at the threshold determined in Fig.2a.

Note that the ice floes surrounded by blue circles are not analyzed correctly. In such cases, manual corrections of ice edges were made.

Figure 3: The cumulative number distribution of floe diameter $N(d)$.

Three kinds of datasets by a ship, a heli, and satellite are compiled to draw this graph. The two lines indicate the two regimes.

Figure 4: The properties of the shape of individual ice floes.

(a) The relationship between diameters d and d_p, obtained from area and perimeter, respectively. The ratio d_p/d is an index of distortion from a circle.

(b) The relationship between maximum (d_{max}) and minimum (d_{min}) caliper diameters.

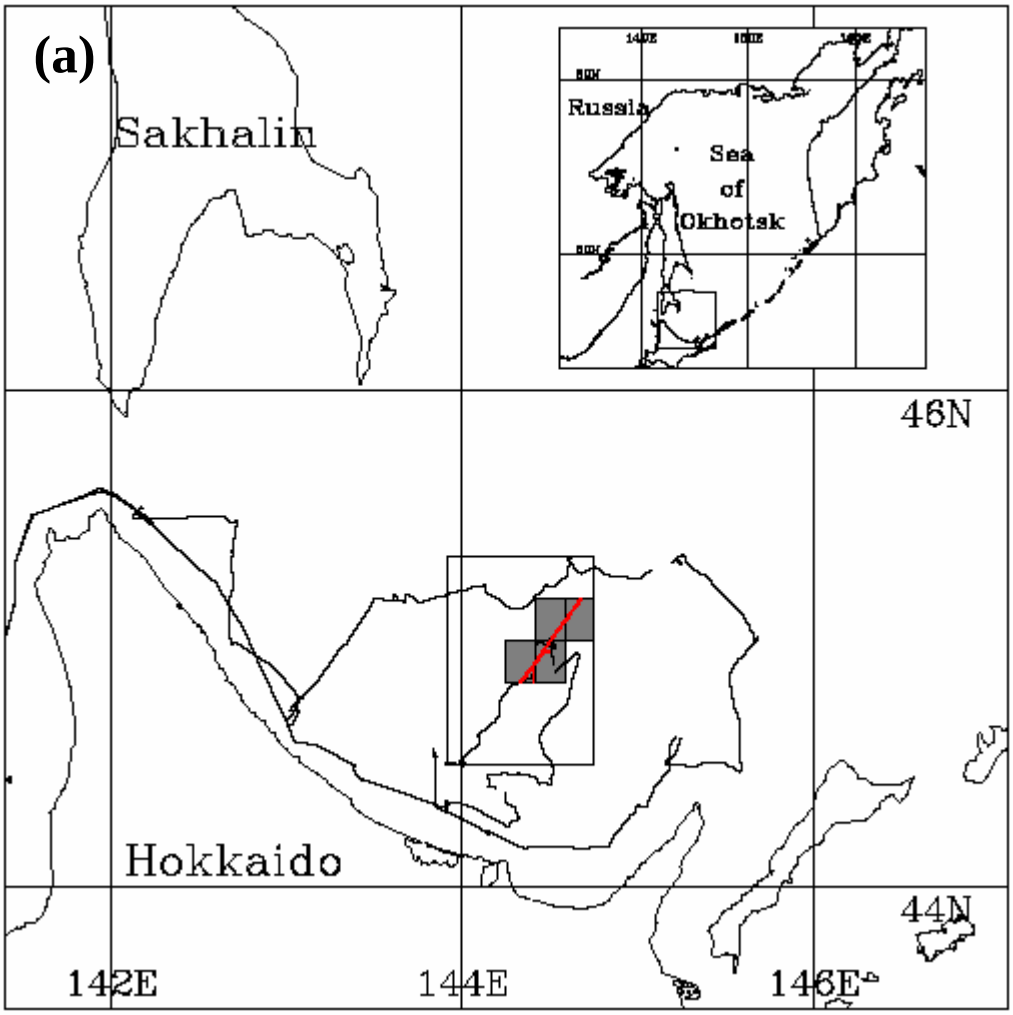
(a)
Sakhalin
Russia
Sea
of
Okhotsk
46N
Hokkaido
44N
142E
144E
146E

Figure 1a

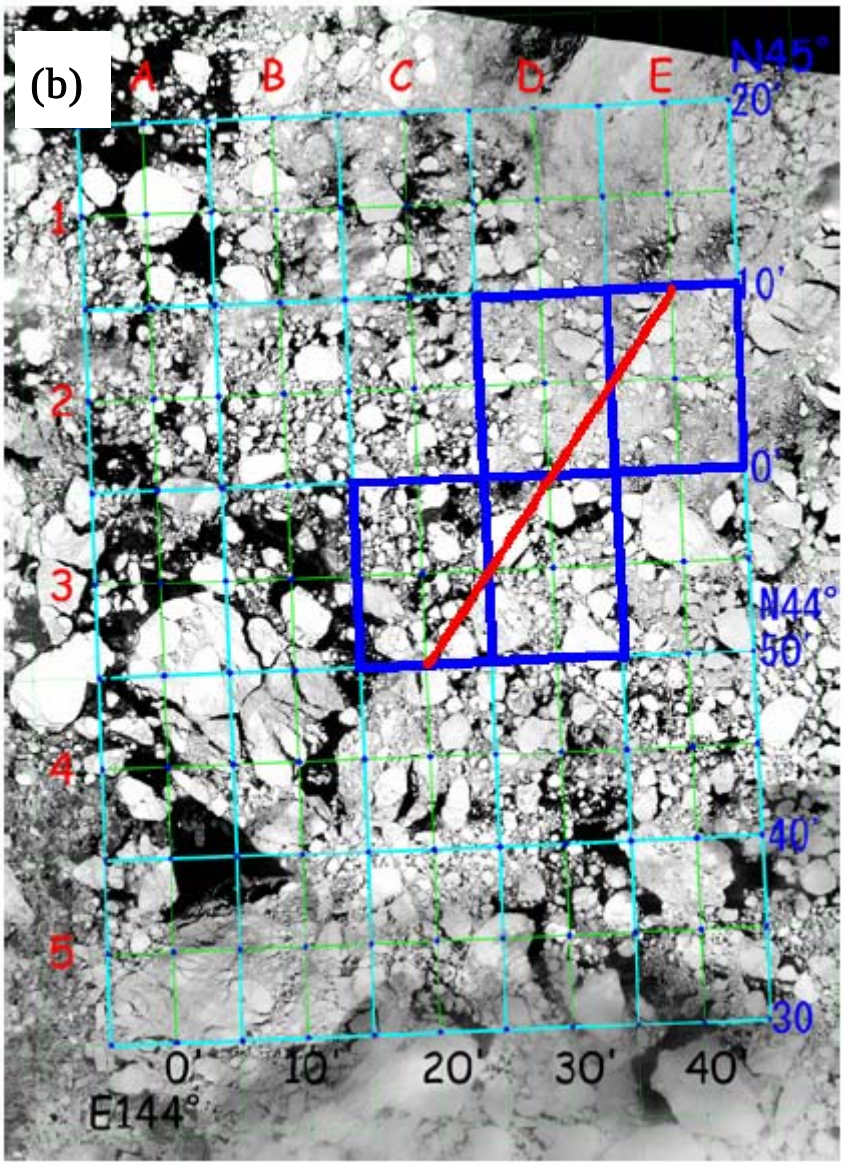

Figure 1b

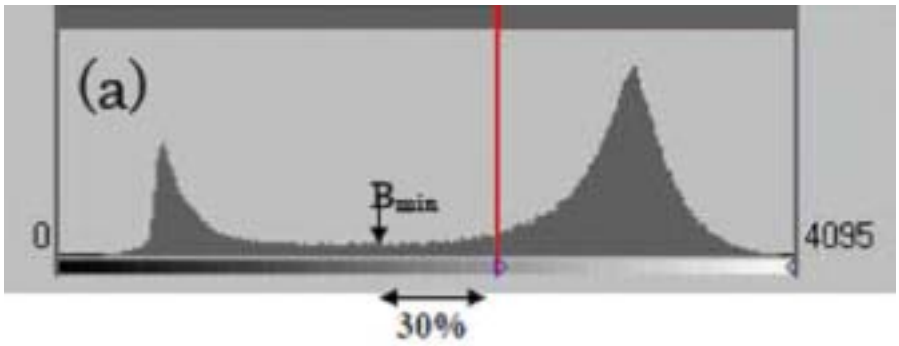

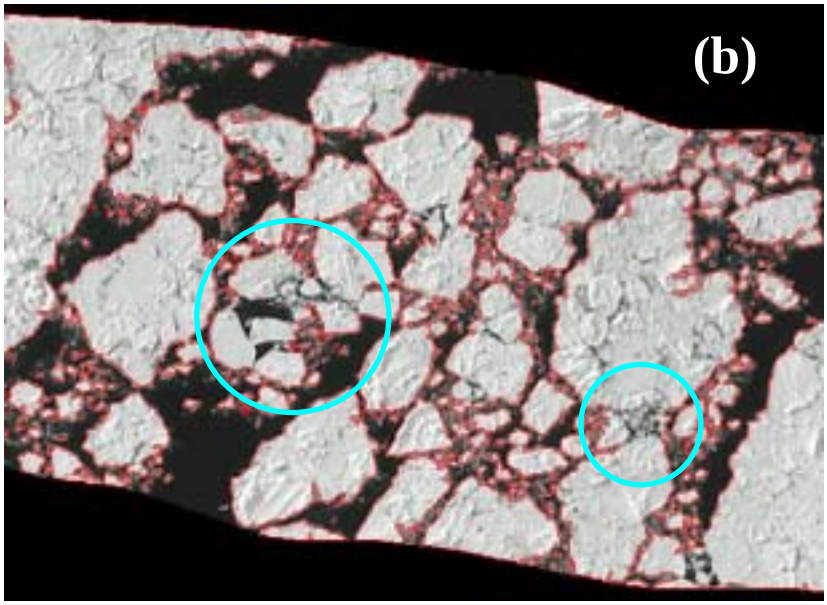

Figure 2

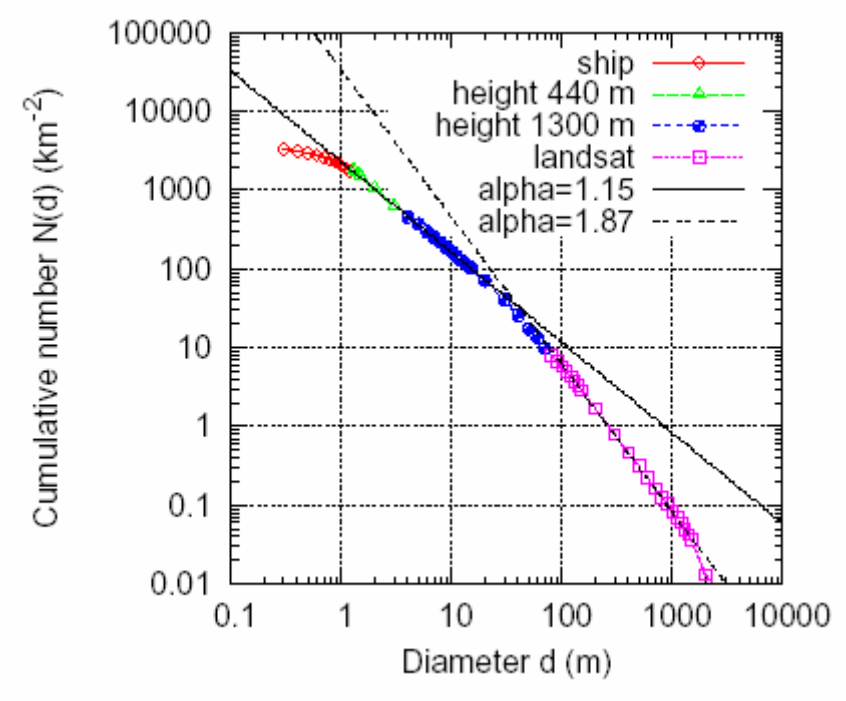
Cumulative number N(d) (km-2)
Diameter d (m)
100000
10000
1000
100
10
1
0.1
0.01
0.1
1
10
100
1000
10000
ship
height 440 m
height 1300 m
landsat
alpha=1.15
alpha=1.87

Figure 3

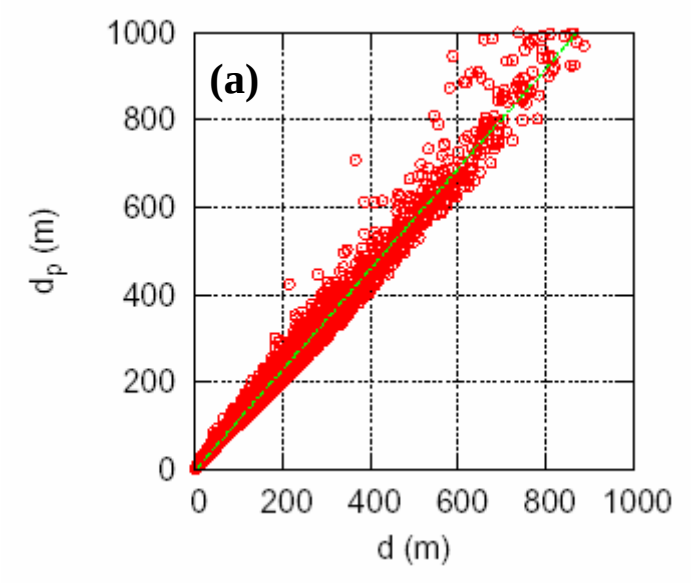
(a)
1000
800
600
400
200
0
0
200
400
600
800
1000
d (m)
d_p (m)

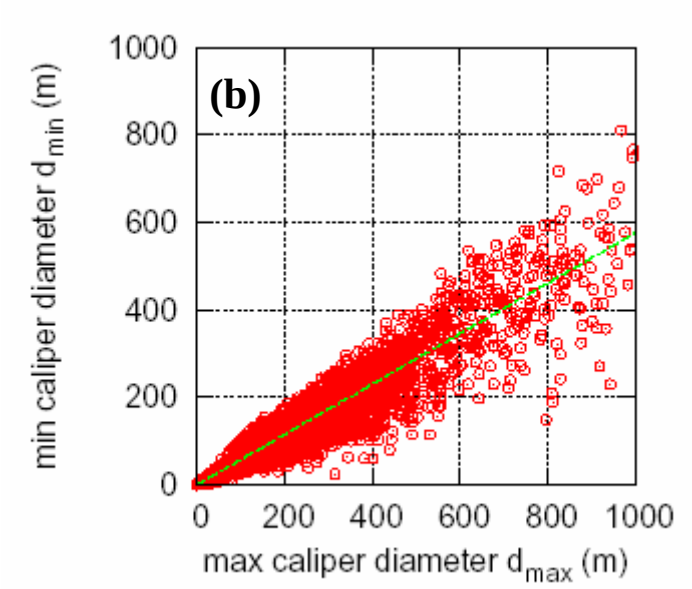
(b)
1000
800
600
400
200
0
0
200
400
600
800
1000
max caliper diameter d_{max} (m)
min caliper diameter d_{min} (m)

Figure 4